nanomaterials

MDPI

Article

Copper Cobalt Sulfide Structures Derived from MOF Precursors with Enhanced Electrochemical Glucose Sensing Properties

Daojun Zhang [1,*], Xiaobei Zhang [1,2], Yingping Bu [1,2], Jingchao Zhang [1] and Renchun Zhang [1]

[1] College of Chemistry and Chemical Engineering, Anyang Normal University, Anyang 455000, China; zzuczxb@126.com (X.Z.); m18337278507@163.com (Y.B.); zjc19830618@126.com (J.Z.); rczhang@aynu.edu.cn (R.Z.)
[2] College of Chemistry, Zhengzhou University, 100 Science Road, Zhengzhou 450001, China
* Correspondence: zhangdj0410@sohu.com; Tel.: +86-372-2900040

Abstract: Nonenzymatic electrochemical detection of glucose is popular because of its low price, simple operation, high sensitivity, and good reproducibility. Co-Cu MOFs precursors were synthesized via the solvothermal way at first, and a series of porous spindle-like Cu-Co sulfide microparticles were obtained by secondary solvothermal sulfurization, which maintained the morphology of the MOFs precursors. Electrochemical studies exhibit that the as-synthesized Cu-Co sulfides own excellent nonenzymatic glucose detection performances. Compared with CuS, Co (II) ion-doped CuS can improve the conductivity and electrocatalytic activity of the materials. At a potential of 0.55 V, the as-prepared Co-CuS-2 modified electrode exhibits distinguished performance for glucose detection with wide linear ranges of 0.001–3.66 mM and high sensitivity of 1475.97 $\mu A \cdot mM^{-1} \cdot cm^{-2}$, which was much higher than that of CuS- and Co-CuS-1-modified electrodes. The constructed sulfide sensors derived from MOF precursors exhibit a low detection limit and excellent anti-interference ability for glucose detection.

Keywords: copper cobalt sulfide; porous structures; nonenzymatic glucose sensing; electrocatalysts

Citation: Zhang, D.; Zhang, X.; Bu, Y.; Zhang, J.; Zhang, R. Copper Cobalt Sulfide Structures Derived from MOF Precursors with Enhanced Electrochemical Glucose Sensing Properties. *Nanomaterials* **2022**, *12*, 1394. https://doi.org/10.3390/nano12091394

Academic Editor: Jung Woo Lee

Received: 4 March 2022
Accepted: 7 April 2022
Published: 19 April 2022

1. Introduction

Currently, diabetes as a common chronic disease is already a serious threat to human health. Therefore, developing a simple and sensitive detection method for glucose is important for clinical diagnosis and diabetes management [1,2]. Compared with colorimetry, spectroscopy, and fluorescence analytical methods, nonenzymatic electrochemical glucose detection has received widespread attention due to its low cost, simple operation, and high sensitivity [3–5]. In recent years, transition-metal oxides (TMOs) and transition-metal sulfides (TMSs) have been exploited as advanced electrocatalysts to construct high performance electrochemical sensors [6–19].

Recently, among the transition-metal based electrodes materials, copper-based oxides and sulfides with various morphologies and structures have been used as electrode materials for nonenzymatic electrochemical glucose detection. For instance, Cu/Cu_2O hollow microspheres were prepared by solvothermal conditions and exhibited a high catalytic activity for glucose oxidation [20]. The glucose electrochemical sensor constructed by CuO nanorod dispersed hollow carbon fibers (CuO NR @ PCFs) [21] showed a wide linear range (0.005–0.8 mM, 0.8–8.5 mM) and a low detection limit (0.1 μM). The reported flower-like $CuCo_2O_4/C$ microspheres [22] -constructed sensor exhibited a wide linear range and low detection limit. The $Cu_xCo_{3-x}O_4$ nano-needle framework thin-film electrode reported by Xu [23] exhibited an ultrahigh sensitivity of 13,291.7 $\mu A \cdot mM^{-1} \cdot cm^{-2}$ for glucose detection. CuS nanotubes were prepared in an O/W microemulsion system at low temperature [24], and the glucose concentration could be detected by the CuS nanotube sensor with high sensitivity (7.842 $\mu A \cdot \mu M^{-1}$). Karikalan et al. synthesized S-rGO/CuS nanocomposites to construct an electrochemical glucose sensor, and the linear concentration range of the

constructed sensor was 0.0001–3.88 mM and 3.88–20.17 mM, respectively, and the detection limit of 32 nM was quite low [25]. Xu et al. demonstrated the synthesis of $CuCo_2S_4$ nanosheets on flexible carbon fiber textiles (CFT) by a hydrothermal method [26]. The sensor constructed of $CuCo_2S_4$ nanosheets had a high sensitivity of 3852.7 $\mu A \cdot mM^{-1} \cdot cm^{-2}$ and a linear range up to 3.67 mM. Compared with related transition metal oxides, copper cobalt sulfides are more suitable as electrode materials for nonenzymatic glucose sensors due to the improved electrical conductivity [26].

In recent years, metal−organic frameworks (MOFs) have served as self-sacrificial precursors for preparation of porous micro-/nanostructured transition metal oxides and sulfides [27–30]. The MOF-derived TMOs and TMSs usually exhibit porous structures and high surface areas with enhanced electrocatalytic and electrochemical energy storage performances [31–35]. In this work, the shuttle-like copper cobalt sulfide structures were synthesized via MOF sacrificial templates. The electrochemical properties of copper cobalt sulfide -constructed electrodes were studied by cyclic voltammetry and the amperometric method. At a potential of 0.55 V, the linear range of Co-CuS-2 modified electrode was 0.001–3.66 mM with a detection limit of 0.1 μM, and the sensitivity of the electrode was 1475.97 $\mu A \cdot mM^{-1} \cdot cm^{-2}$. The results indicate that the sensor owns good electrochemical sensing performance for glucose and has a potential application in glucose detection.

2. Experimental Section

2.1. Chemicals

Polyvinylpyrrolidone (PVP) and 2,5-dihydroxyterephthalic acid (H_4dobdc) were purchased from Shanghai Macklin Biochemical Co., Ltd. (Shanghai, China); $Cu(NO_3)_2 \cdot 4H_2O$, $Co(NO_3)_2 \cdot 6H_2O$, glucose (Glu), ascorbic acid (AA), and NaOH were purchased from Sinopharm Chemical Reagent Co., Ltd. (Shanghai, China); Thioacetamide (TAA), uric acid (UA), dopamine (DA), sodium chloride (NaCl), glutathione (GSH), and sucrose (Suc) were purchased from Aladdin Industrial Corporation (Shanghai, China); Ethylene glycol, ethanol, and N,N-dimethylformamide (DMF) were purchased from Tianjin Fuyu Fine Chemical Co., Ltd. (Tianjin, China). All chemicals and solvents were used without further purification.

2.2. Preparation of Spindle-like Cu-Co Sulfide Microparticles

The solvent system of Cu-Co MOF precursors synthesis is similar to that of our previously reported paper [36]. For the preparation of Co-Cu MOF precursors, $Cu(NO_3)_2 \cdot 4H_2O$, $Co(NO_3)_2 \cdot 6H_2O$, 2,5-dihydroxyterephthalic acid (H_4dobdc), and polyvinylpyrrolidone (PVP) were added in DMF/ethanol/water mixed solvent according to the molar ratio of Co/Cu of 8:2, 7:3 and 0:1, the mixture was heated at 100 °C for 12 h, and then MOF precursors were isolated and washed twice with DMF and water. Cu-Co sulfides were synthesized via an effective sulfurization treatment of MOF precursors with thioacetamide (TAA), the samples with Co/Cu ratio from high to low denoted as Co-CuS-1 and Co-CuS-2, respectively. The MOF precursors were redispersed into 3 mL of ethylene glycol. Then, 0.0043 g of TAA was added and fully stirred, the mixture was transferred into a 25 mL stainless-steel Teflon-lined autoclave and reacted at 110 °C for 12 h, and the black powder was obtained and washed three times with ethanol and water.

2.3. Materials Characterization

Powder X-ray diffraction (PXRD) analyses of the as-prepared samples were conducted on a PANalytical X'Pert PRO MPD system with Cu_{Ka} radiation (λ = 1.5418 Å) and operated at 40 kV and 40 mA. The morphologies and compositions were analyzed by scanning electron microscopy (SEM) with energy dispersive spectroscopy (EDS) on a Hitachi SU-8010 instrument and X-ray photo-electron spectroscopy (XPS) using Thermo-Scientific system. The specific surface areas of the samples were acquired by N_2 adsorption/desorption isotherms measured on a Gemini VII 2390 analyzer at 77 K.

2.4. Electrode Preparation and Measurement

All electrochemical tests were conducted on a CHI660E electrochemical workstation with a typical three-electrode system. First, 2 mg Co-Cu sulfides was dispersed in 1.0 mL distilled H_2O via ultrasound 30 min. A glassy carbon electrode (GCE) with diameter 3 mm was polished with alumina slurries and washed with ultrapure H_2O. Afterward, 5 μL of the suspension was covered onto the GCE surface to obtain Co-CuS/GCE. The modified electrode was used as the working electrode, Ag/AgCl was used as the reference electrode, and Pt wire was used as the counter electrode.

3. Results and Discussion

The morphologies of Co-Cu MOF precursors were analyzed by scanning electron microscopy (SEM) technique and are shown in Figure 1, which exhibited a spindle-like structure with a well-distributed and smooth surface. Figure 2 shows the SEM images of derived samples of CuS (Figure 2a,b), Co-CuS-1 (Figure 2d) and Co-CuS-2 (Figure 2e). After effective sulfurization treatment of MOF precursors with TAA, the derived products can largely retain the morphology of MOF precursors; however, the surface of all samples seems rough and porous. According to the EDS mapping images of a single shuttle-like CuS particle (Figure 2c), the Cu and S elements are evenly distributed. Figures S1 and 2f show the EDS mapping images of Co-CuS-1 and Co-CuS-2, respectively. It can be seen from the images that there is a distribution of Co, Cu and S elements, which indicates that Co element is doped into CuS microparticles. The phase of as-synthesized sulfides was checked by the XRD patterns and are exhibited in Figure 3a; all the positions of the peaks are consistent with the standard card number JCPDS No.065-3588 of the hexagonal phase CuS, and no other impurity peaks appear in the patterns. It can be deduced that partial-doped cobalt ions into CuS do not change its crystal structure. Figure 3b shows the N_2 adsorption isotherm of the Co-CuS-2 sample and the corresponding pore size distribution. Co-CuS-2 is the type IV adsorption isotherm, which belongs to the typical mesoporous structure. The specific surface area calculated by the BET method is 16.3 $m^2\ g^{-1}$, and the average pore size is 31.72 nm. The element content of the Co-CuS-1 and Co-CuS-2 samples were further characterized by EDS, which indicated that the Co/Cu ratios are close to the stoichiometric ratio of raw materials (Figure 4a). XPS technique was further used to analyze the surface valance state of Co and Cu in the corresponding sulfide. Figure S2 provides the XPS survey spectra of the as-synthesized samples. The high revolution spectra are shown in Figure 4b–d. The high revolution spectra of Cu in the three samples are similar, the binding energy of the two peaks located at 931.4 and 951.3 eV was attributed to Cu $2p_{3/2}$ and Cu $2p_{1/2}$, respectively [25]. The fitted peaks of 931.4 and 951.2 eV indicate the existence of Cu^+, and the peaks at 932.4 and 953.1 eV correspond to Cu^{2+}. The high resolution Co 2p spectra in Co-CuS-1 are fitted with two doublet peaks centered at 780.5 and 796.4 eV, which correspond to Co^{3+}. The peaks at 781.9 and 797.5 eV correspond to Co^{2+}. Figure 4d shows the S 2p spectra, with the peaks centered at 161.2 and 162.4 eV for S $2p_{3/2}$ and S $2p_{1/2}$, respectively. For Co-CuS-2, the peak of 163.6 eV increased dramatically, which can be ascribed to a Metal-S bond at a low coordination environment and contributed to an increase in the intrinsic conductivity [37,38].

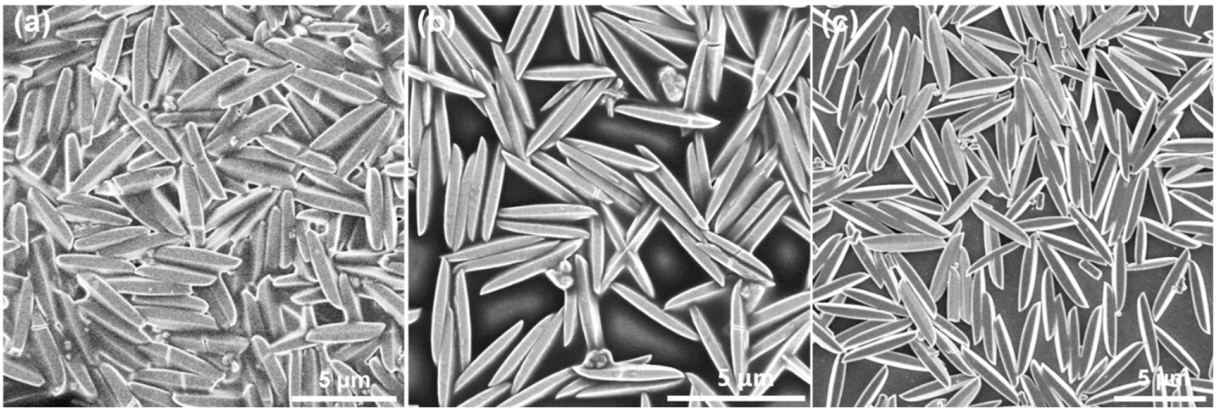

Figure 1. SEM images of (**a**) Cu-MOF, (**b**) CuCo-MOF-1, and (**c**) CuCo-MOF-2 precursors.

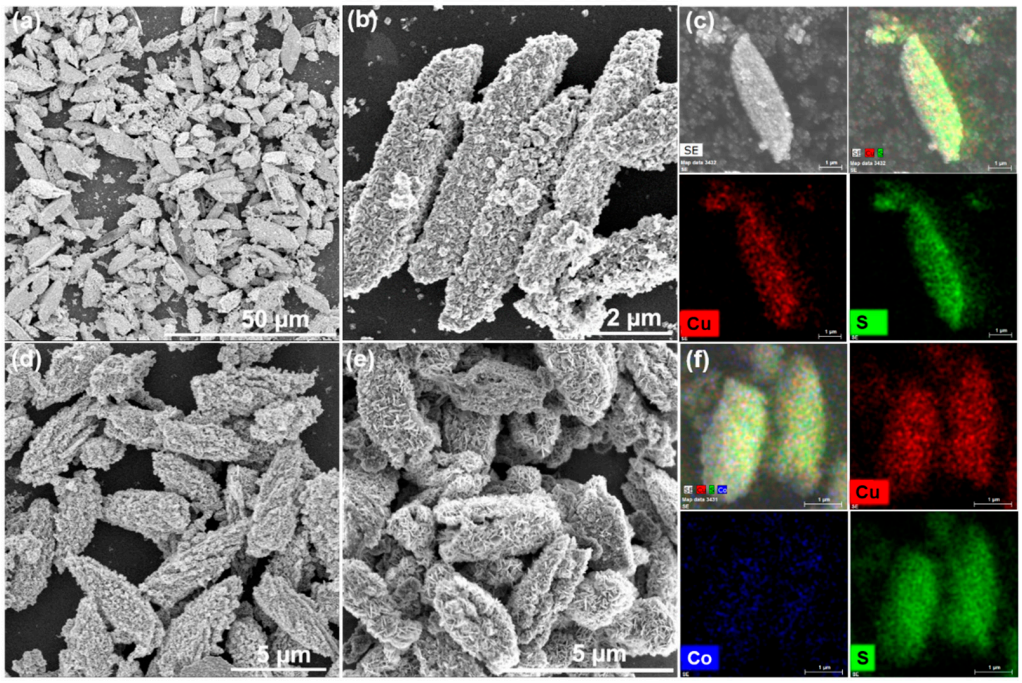

Figure 2. SEM images of copper cobalt sulfides (**a**,**b**) CuS, (**d**) Co-CuS-1, (**e**) Co-CuS-2, and the EDX mapping element distribution of (**c**) CuS, (**f**) Co-CuS-2.

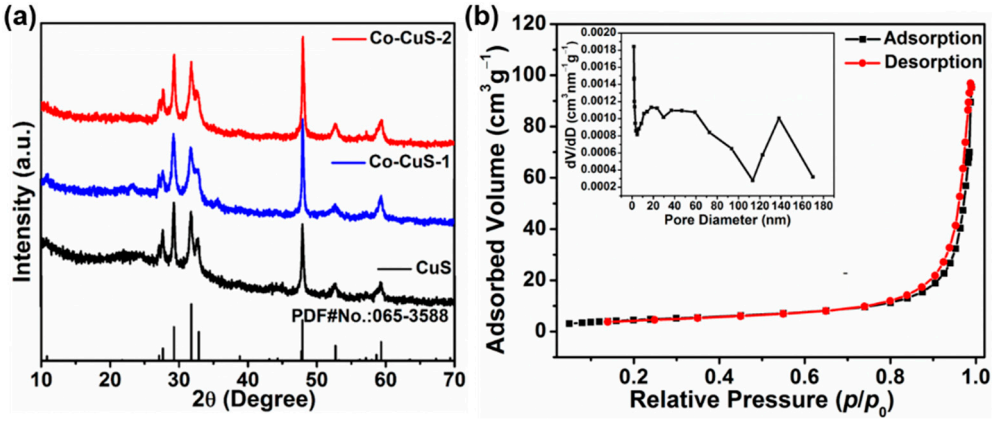

Figure 3. (**a**) XRD patterns of the samples with different proportions; (**b**) N_2 adsorption isotherm and pore distribution of Co-CuS-2.

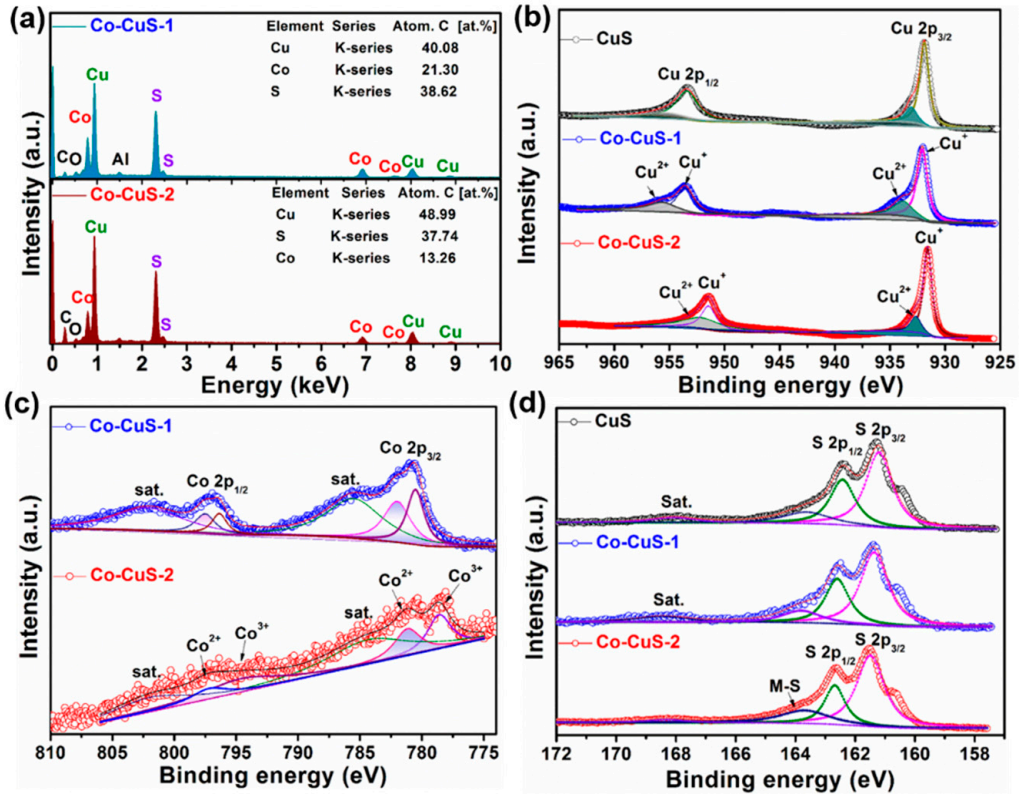

Figure 4. (**a**) EDS of CuS-1 and Co-CuS-2 samples. High resolution XPS spectra of Cu (**b**), Co (**c**), and S (**d**) for CuS, Co-CuS-1, and Co-CuS-2 samples.

Figure 5a shows the CV curves of the bare electrode and copper cobalt sulfide-modified electrodes in the 0.1 M NaOH electrolyte containing 1 mM Glu. As shown in Figure 5a, the bare electrode has almost no response, CuS- and Co-CuS-1-modified electrodes have weak redox peaks, and the Co-CuS-2-modified electrode has a pair of obvious redox peaks at 0.45/0.60 V (vs. Ag/AgCl), indicating that the Co-CuS-2 sample exhibits the best response to glucose. As shown in Figure 5b–d, the CV curves of CuS, Co-CuS-1, and Co-CuS-2 at different glucose concentrations further show that the redox peaks of the Co-CuS-2 electrode is the strongest, indicating that this material has the best electrocatalytic performance for glucose among the three samples. The possible oxidation mechanism of glucose may be described in the following three steps [22,23,26]:

$$\mathrm{CuCo\text{-}S} + \mathrm{OH^-} + \mathrm{H_2O} \rightarrow \mathrm{CuSOH} + \mathrm{CoSOH} + \mathrm{e^-} \quad (1)$$

$$\mathrm{CoSOH} + \mathrm{OH^-} \rightarrow \mathrm{CoSO} + \mathrm{H_2O} + \mathrm{e^-} \quad (2)$$

$$\mathrm{CuOSH} + \mathrm{CoSO} + \mathrm{glucose} \rightarrow \mathrm{CuS} + \mathrm{CoSOH} + \mathrm{glucolactone} \quad (3)$$

CuSOH and CoSO intermediator might be formed through electrooxidation at alkaline conditions. The formed CuSOH and CoSO adsorbed glucose molecules and subsequently oxidated to gluconolactone in an alkaline medium.

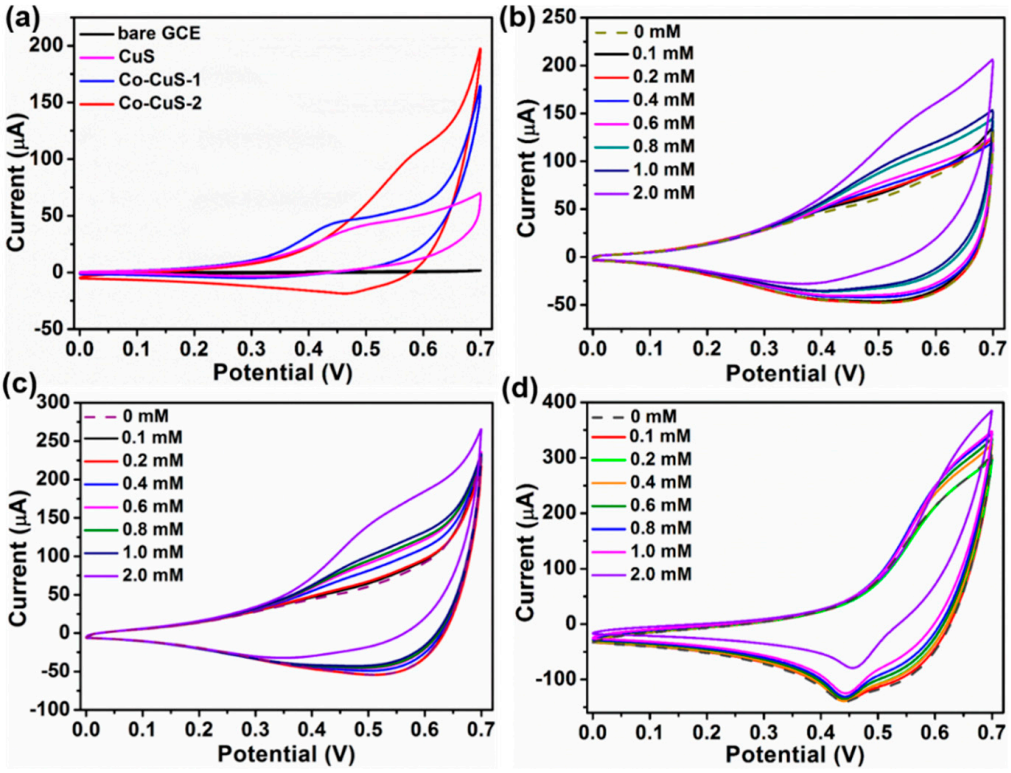

Figure 5. (**a**) CV curves of CuS, Co-CuS-1, Co-CuS-2 and bare electrode in 0.1 M NaOH electrolyte containing 1 mM Glu (20 mV·s^{-1}). CV curves in NaOH solution with different glucose concentration: (**b**) CuS, (**c**) Co-CuS-1, and (**d**) Co-CuS-2 (100 mV·s^{-1}).

In order to further acquire the kinetic information of glucose electrocatalytic oxidation of the CuS, Co-CuS-1, and Co-CuS-2 electrodes, the CV curves of three samples at scan rates varying from 20 to 180 mV·s^{-1} were studied. Figure 6a,c,e shows the CV curves of CuS, Co-CuS-1, and Co-CuS-2 in 0.1 M NaOH solution containing 1 mM glucose at different scan rates. The peak current of the three samples increases steadily with the increase in scan rate. As seen in Figure 6b,d, the peak current (anodic and cathodic) of the CuS and Co-CuS-1 electrodes increases linearly with the scan rate, and the fitted linear equations are $I_{pa} = 0.626v + 31.172$, $I_{pc} = -0.489v + 12.852$, and $I_{pa} = 0.634v + 28.708$, $I_{pc} = -0.717v + 17.782$ respectively, indicating that CuS and Co-CuS-1 electrodes are adsorption-controlled processes for oxidation glucose. Figure 6f shows that both the anodic and cathodic peak current has a linear relationship with the square root of the scan rate, indicating that Co-CuS-2 is a diffusion-controlled process. The fitted linear equations are $I_{pa} = 21.176v^{1/2} + 47.474$, $I_{pc} = -15.716v^{1/2} + 8.971$, respectively, and this may be attributed to the large surface area and good conductivity; thus, it is conducive to glucose detection.

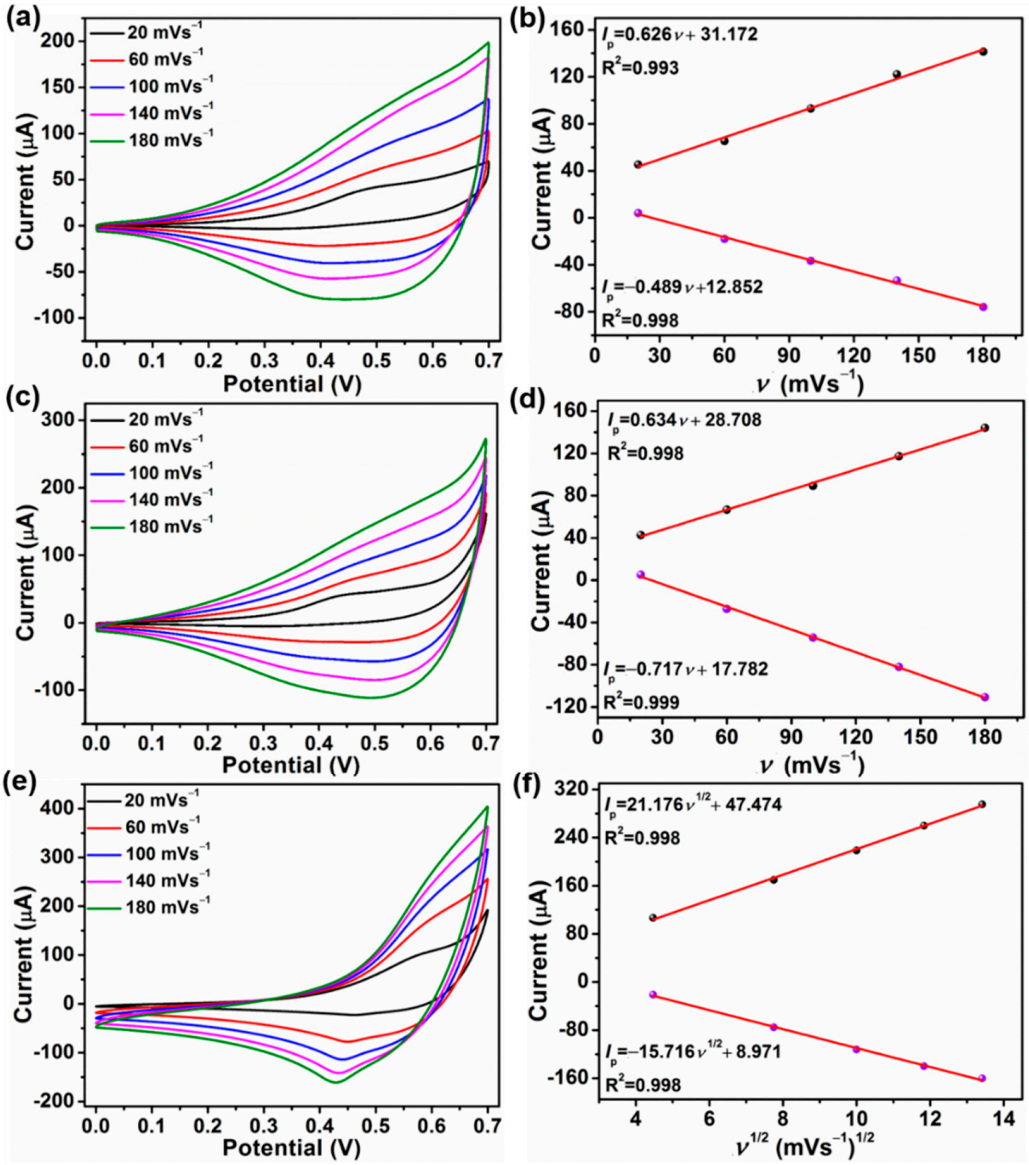

Figure 6. CV curves at different scan rates (20–180 mV s^{-1}) in a 1 mM glucose solution (**a**) CuS, (**c**) Co-CuS-1, (**e**) Co-CuS-2, and the corresponding linear calibration curves, (**b**) CuS, (**d**) Co-CuS-1, (**f**) Co-CuS-2, respectively.

In order to systematically study the effect of working potential on the electrocatalytic oxidation of glucose for CuS-, Co-CuS-1-, and Co-CuS-2-modified electrodes, the current−time (*I*–t) curves at different potentials were measured. Figure 7a shows the current response (0.1 M NaOH) of the CuS electrode via a continuously increasing glucose concentration at 0.5, 0.55 and 0.6 V. The CuS electrode exhibits the highest amperometric response at 0.6 V. The corresponding calibration curve at 0.6 V is also shown in Figure 7b. The linear range of the CuS electrode is 0.002–2.16 mM, the sensitivity is 905.42 μA·mM^{-1}·cm^{-2}, and the limit of detection (LOD) of 0.9 μM is calculated based on 3σ/s, where σ is the standard deviation of the blank, and s is the slope of the calibration curve [12,39].

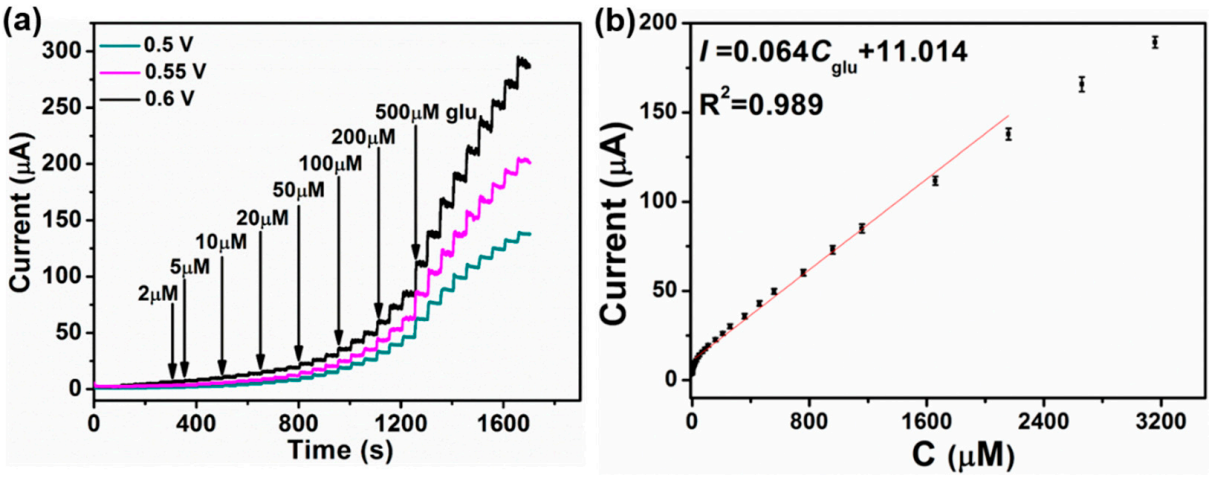

Figure 7. (**a**) Current−time curves of the CuS electrode with the continuous addition of glucose solution at 0.5, 0.55 and 0.6 V (0.1 M NaOH), respectively. (**b**) The calibration curves fitted from the current responses at 0.6 V.

Figure 8a,b shows the *I*–t curves of Co-CuS-1 and Co-CuS-2 at different potentials, which shows the best glucose electrocatalytic performance at a potential of 0.55 V after Co doping. Thus, the electrocatalytic properties of CuS, Co-CuS-1 and Co-CuS-2 at 0.55 V were compared and are shown in Figure 8c. It can be seen from the image that the amperometric response of Co-CuS-2 is the highest. Figure 8d shows the calibration curve of CuS at 0.55 V; the linear range is 0.002–2.66 mM, the sensitivity is 686.13 $\mu A \cdot mM^{-1} \cdot cm^{-2}$, and the detection limit is 0.4 μM (3σ/s). Figure 8e shows the calibration curve of Co-CuS-1; the linear range is 0.001–3.16 mM, the sensitivity increases to 1206.75 $\mu A \cdot mM^{-1} \cdot cm^{-2}$, and the detection limit decreases to 0.3 μM (3σ/s). Figure 8f shows the calibration curve of Co-CuS-2 at 0.55 V; the linear range extends from 0.001 mM to 3.66 mM, the sensitivity is 1475.97 $\mu A \cdot mM^{-1} \cdot cm^{-2}$, and the detection limit is 0.1 μM (3σ/s). Table 1 shows the details. As compared, at a potential of 0.55 V, Co-CuS-2 has the widest linear range, the highest sensitivity and lowest LOD among the three electrodes. The sensitivity of the Co-CuS-2 sensor is higher than that of the Cu/Cu_2O hollow microspheres [20], $CuCo_2O_4/C$ microspheres [22], hierarchical Co_3O_4 film [39], CuO_x-CoO_x/graphene [40], Octahedral Cu_2O [41], and CuO microspheres [42]; however, it is lower than that of the $CuCo_2S_4$ nanosheets [26] and $NiCo_2O_4$ hollow nanorods [43]. The comprehensive performance of Co-CuS-2/GCE is equivalent to or better than that of previously reported electrochemical glucose sensors (Table 2).

Table 1. Electrochemical sensing properties of Cu-Co sulfides with different doping ratios.

Electrode Material	Potential (V)	Linear Range (mM)	Detection Limit (μM)	Sensitivity ($\mu A \cdot mM^{-1} \cdot cm^{-2}$)
CuS	0.55	0.002–2.66	0.4	686.13
	0.60	0.002–2.16	0.9	905.42
Co-CuS-1	0.55	0.001–3.16	0.3	1206.75
Co-CuS-2	0.55	0.001–3.66	0.1	1475.97

Table 2. Comparison of the Co-CuS-2 electrode with some reported sensors for glucose detection.

Electrode Material	Potential (V)	Linear Range (mM)	Detection Limit (μM)	Sensitivity ($\mu A \cdot mM^{-1} \cdot cm^{-2}$)	Ref.
Co-CuS-2	0.55	0.001–3.66	0.1	1475.97	This work
Cu/Cu_2O hollow microspheres	0.45	0.22–10.89	0.05	33.63 $\mu A \cdot mM^{-1}$	20

Table 2. *Cont.*

Electrode Material	Potential (V)	Linear Range (mM)	Detection Limit (μM)	Sensitivity ($\mu A \cdot mM^{-1} \cdot cm^{-2}$)	Ref.
CuO NR @ PCFs	0.60	0.005–0.8 0.8–8.5	0.1	608	21
$CuCo_2O_4$/C microspheres	0.60	0.005–8	1.5	707.71	22
CuS nanotube	0.20	0.05–5	–	7.842 $\mu A \cdot mM^{-1}$	24
$CuCo_2S_4$/carbon fiber textile	0.35	up to 3.67	1.01	3852.7	26
Co_3O_4 porous film	0.6	up to 3.0	1	366.03	39
CuO_x-CoO_x/ graphene	0.50 (vs. SCE)	0.005–0.57	0.5	507	40
Octahedral Cu_2O	0.60	0.3–4.1	128	241	41
CuO microspheres	0.45 (vs. SCE)	0.001–4	0.5	349.6	42
$NiCo_2O_4$ hollow nanorods	0.60	0.0003–1	0.16	1685.1	43

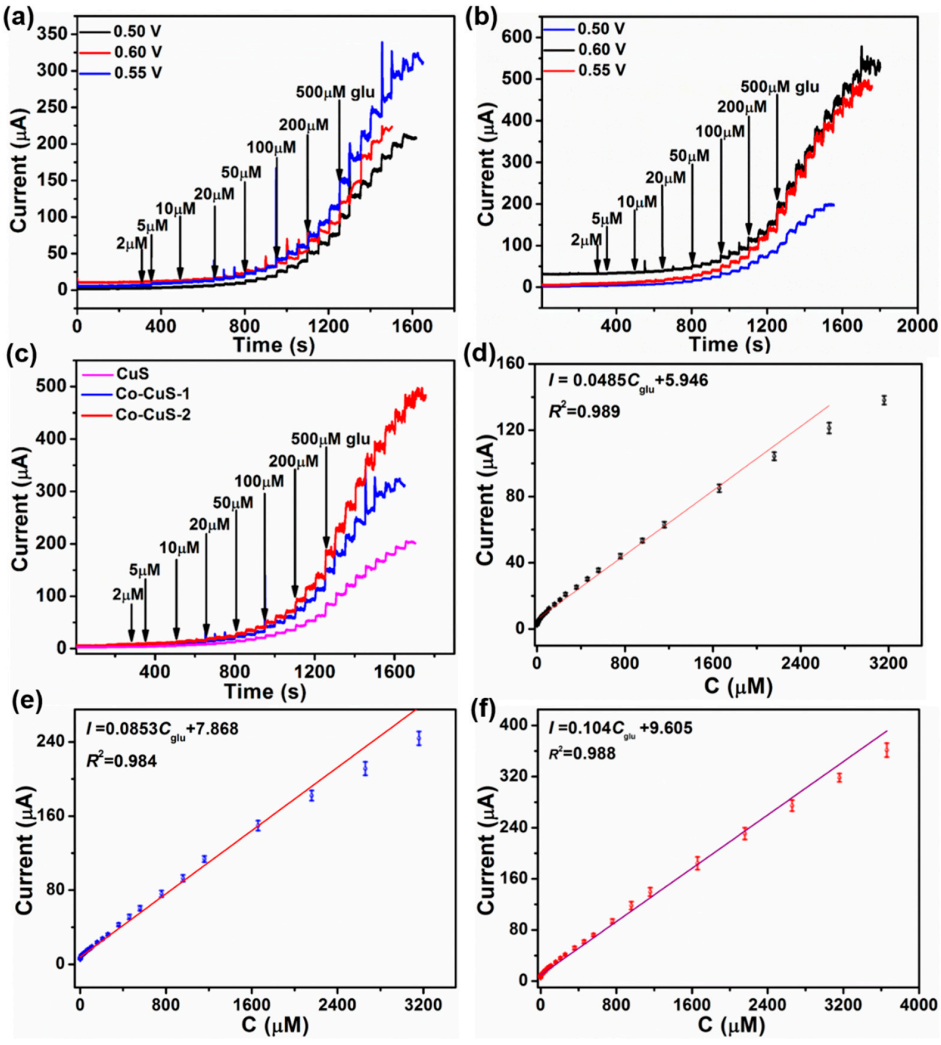

Figure 8. Current response of continuously increasing glucose concentration at 0.5, 0.55 and 0.60 V (0.1 M NaOH): (**a**) Co-CuS-1, (**b**) Co-CuS-2, (**c**) current response of CuS, Co-CuS-1 and Co-CuS-2 at 0.55 V. The corresponding calibration curves at 0.55 V: (**d**) CuS, (**e**) Co-CuS-1, (**f**) Co-CuS-2.

As shown in Figure 9a, all Nyquist diagrams contain the semicircular part at high frequency and the oblique line at low frequency. The tilt line is related to the diffusion limit step, and the R_{ct} of the electrode surface can be equal to the radius of the semicircular part. The radius of Co-CuS-2 is the smallest, indicating that the conductivity of Co-CuS-2 is the largest, which is one of the reasons for its best electrocatalytic performance for glucose. The repeatability of CuS, Co-CuS-1 and Co-CuS-2 electrodes were tested and are shown in Figure 9b. The current response of adding 200 μM Glu 13 times in 0.1 M NaOH solution at a potential of 0.55 V shows that the current response of Co-CuS-2 is high, the step change is almost unchanged, and the calculated RSD is 4.19%. In order to evaluate the selectivity of the constructed electrodes to glucose detection, as shown in Figure 9c, three different sulfide electrodes showed good anti-interference performance at a working potential of 0.55 V. The specific operation is to add 200 μM glucose (Glu), 20 μM ascorbic acid (AA), uric acid (UA), dopamine (DA), sodium chloride (NaCl), glutathione (GSH), sucrose (Suc) and 200 μM glucose (Glu) in 0.1 M NaOH supporting solution. It can be seen from the *I*–t curves that the response current for glucose of the Co-CuS-2-modified electrode remains unchanged after adding interfering substances, while the response current of interferents is almost negligible, indicating that the electrode has good selectivity for glucose detection. Figure 9d shows the stability of the as-synthesized sample-modified electrodes. After adding 200 μM Glu solution, the current response lasts for 3500 s. The results show that the retention rates of Co-CuS-2, Co-CuS-1 and CuS are 93%, 76% and 84%, respectively, indicating that Co-CuS-2 has the best stability. Therefore, the Co-CuS-2-modified electrode has good reproducibility, selectivity, and stability for the detection of glucose.

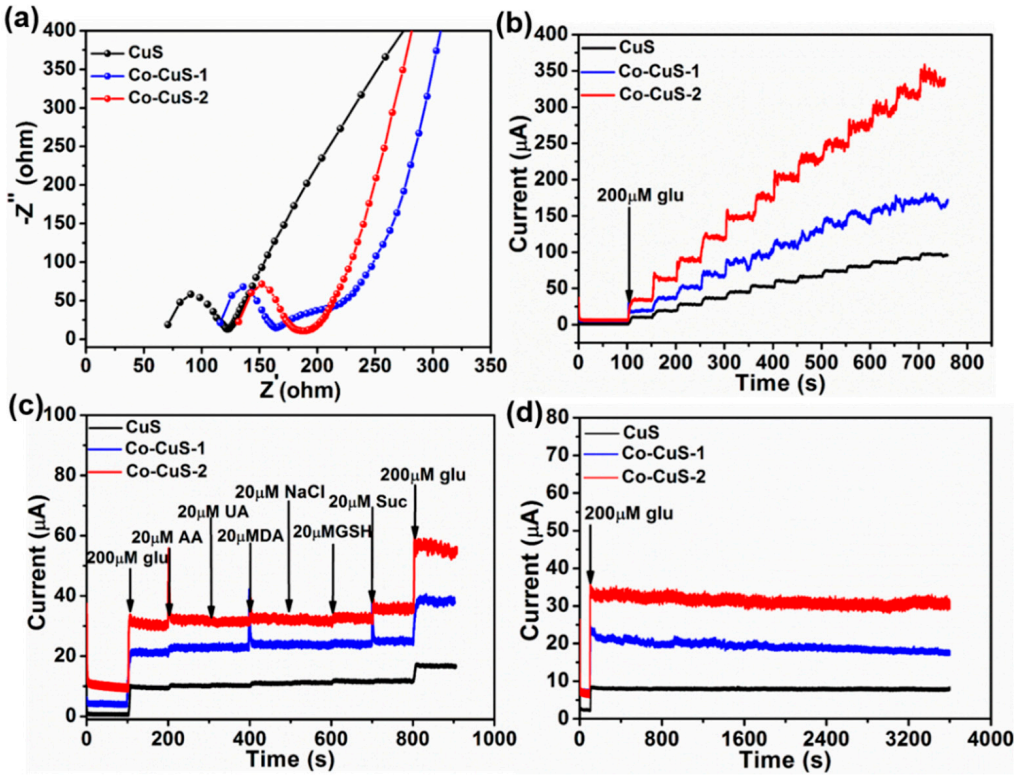

Figure 9. (**a**) Impedance diagram of CuS, Co-CuS-1 and Co-CuS-2 samples, (**b**) reproducibility, (**c**) anti-interference, and (**d**) stability.

4. Conclusions

Co/Cu MOFs precursors were synthesized by the one-step solvothermal method, and a series of porous spindle-like Cu-Co sulfide microparticles were obtained by secondary solvothermal sulfurization, which maintained the morphology of the MOFs precursors. The porous structure of these materials was conducive to the diffusion of electrolytes

and analytes. Compared with CuS, Co (II) ion doping can improve the conductivity and electrocatalytic activity of the materials. At a potential of 0.55 V, the linear range of the Co-CuS-2 electrode for glucose detection was 0.001–3.66 mM with an LOD of 0.1 μM, and the sensitivity was 1475.97 $\mu A \cdot mM^{-1} \cdot cm^{-2}$, which was much better than that of the CuS and Co-CuS-1 samples. This work provides an effective strategy for glucose detection and opens up a new way to improve the electrochemical performance of non-enzyme electrochemical sensors.

Supplementary Materials: The following supporting information can be downloaded at: https://www.mdpi.com/article/10.3390/nano12091394/s1, Figure S1: EDX mapping images of Co-CuS-1 sample; Figure S2: XPS survey spectra of (a) CuS-1, (b) Co-CuS-1 and (c) Co-CuS-2 samples.

Author Contributions: Conceptualization, D.Z.; Data curation, X.Z., Y.B. and J.Z.; Formal Analysis, D.Z.; Funding acquisition, D.Z.; Investigation, X.Z. and D.Z.; Methodology, D.Z.; Project administration, D.Z. and R.Z.; Supervision, D.Z.; Writing—original draft, X.Z. and D.Z.; Writing—review & editing, X.Z., D.Z. and J.Z. All authors have read and agreed to the published version of the manuscript.

Funding: This work was supported by the National Science Foundation of China (no. 21603004, U1604119, 21501006), the Science and Technology Research Project of Henan Province (222102240096), and the Program for Innovative Research Team of Science and Technology at the University of Henan Province (18IRTSTHN006).

Institutional Review Board Statement: Not applicable.

Informed Consent Statement: Not applicable.

Data Availability Statement: Not applicable.

Conflicts of Interest: The authors declare no conflict of interest.

References

1. Heller, A.; Feldman, B. Electrochemical Glucose Sensors and Their Applications in Diabetes Management. *Chem. Rev.* **2018**, *108*, 2482–2505. [CrossRef] [PubMed]
2. Steiner, M.; Duerkop, A.; Wolfbeis, O. Optical methods for sensing glucose. *Chem. Soc. Rev.* **2011**, *40*, 4805–4839. [CrossRef] [PubMed]
3. Wang, G.; He, X.; Wang, L.; Gu, A.; Huang, Y.; Fang, B.; Geng, B.; Zhang, X. Non-enzymatic electrochemical sensing of glucose. *Microchim. Acta* **2013**, *180*, 161–186. [CrossRef]
4. Dhara, K.; Mahapatra, D. Electrochemical nonenzymatic sensing of glucose using advanced nanomaterials. *Microchim. Acta* **2018**, *185*, 49. [CrossRef] [PubMed]
5. Dong, Q.; Ryu, H.; Lei, Y. Metal oxide based non-enzymatic electrochemical sensors for glucose detection. *Electrochim. Acta* **2021**, *370*, 137744. [CrossRef]
6. Zhang, Y.; Zhou, Q.; Zhu, J.; Yan, Q.; Dou, S.; Sun, W. Nanostructured Metal Chalcogenides for Energy Storage and Electrocatalysis. *Adv. Funct. Mater.* **2017**, *27*, 1702317. [CrossRef]
7. Guo, Y.; Park, T.; Yi, J.; Henzie, J.; Kim, J.; Wang, Z.; Jiang, B.; Bando, Y.; Sugahara, Y.; Tang, J.; et al. Nanoarchitectonics for Transition-Metal- Sulfide-Based Electrocatalysts for Water Splitting. *Adv. Mater.* **2019**, *31*, 1807134. [CrossRef]
8. Yu, X.; Lou, X. Mixed Metal Sulfides for Electrochemical Energy Storage and Conversion. *Adv. Energy Mater.* **2018**, *8*, 1701592. [CrossRef]
9. Rui, X.; Tan, H.; Yan, Q. Nanostructured metal sulfides for energy storage. *Nanoscale* **2014**, *6*, 9889–9924. [CrossRef]
10. Liu, Y.; Li, X.; Shen, W.; Dai, Y.; Kou, W.; Zheng, W.; Jiang, X.; He, G. Multishelled Transition Metal-Based Microspheres: Synthesis and Applications for Batteries and Supercapacitors. *Small* **2019**, *15*, 1804737. [CrossRef]
11. Kulkarni, P.; Nataraj, S.; Geetha Balakrishna, R.; Nagarajua, D.; Reddy, M. Nanostructured binary and ternary metal sulfides: Synthesis methods and their application in energy conversion and storage devices. *J. Mater. Chem. A* **2017**, *5*, 22040–22094. [CrossRef]
12. Yang, P.; Wang, X.; Ge, C.; Fu, X.; Liu, X.; Chai, H.; Guo, X.; Yao, H.; Zhang, Y.; Chen, K. Fabrication of CuO nanosheets-built microtubes via Kirkendall effect for non-enzymatic glucose sensor. *Appl. Surf. Sci.* **2019**, *494*, 484–491. [CrossRef]
13. Li, M.; Han, C.; Zhang, Y.F.; Bo, X.J.; Guo, L.P. Facile synthesis of ultrafine Co_3O_4 nanocrystals embedded carbon matrices with specific skeletal structures as efficient non-enzymatic glucose sensors. *Anal. Chim. Acta* **2015**, *861*, 25–35. [CrossRef] [PubMed]
14. Kang, M.; Zhou, H.; Zhao, N.; Lv, B. Porous Co_3O_4 nanoplates as an efficient electromaterial for non-enzymatic glucose sensing. *CrystEngComm* **2020**, *22*, 35–43. [CrossRef]

15. Zhang, Y.Y.; Wang, L.; Yu, J.; Yang, H.; Pan, G.X.; Miao, L.F.; Song, Y.H. Three-dimensional macroporous carbon supported hierarchical ZnO-NiO nanosheets for electrochemical glucose sensing. *J. Alloys Compd.* **2017**, *698*, 800–806. [CrossRef]
16. Xiao, X.; Zhang, X.; Zhang, Z.; You, J.; Liu, S.; Wang, Y. Macro-/meso-porous $NiCo_2O_4$ synthesized by template-free solution combustion to enhance the performance of a nonenzymatic amperometric glucose sensor. *Microchimi. Acta* **2020**, *187*, 64. [CrossRef]
17. Yang, Z.; Bai, X.; Zhu, S.; Qi, C. Synthesis of porous Co_3S_4 for enhanced voltammetric nonenzymatic determination of glucose. *Microchim. Acta* **2020**, *187*, 98. [CrossRef]
18. Huo, H.; Zhao, Y.; Xu, C. 3D Ni_3S_2 nanosheet arrays supported on Ni foam for high-performance supercapacitor and nonenzymatic glucose detection. *J. Mater. Chem. A* **2014**, *2*, 15111–15117. [CrossRef]
19. Guo, Q.; Wu, T.; Liu, L.; He, Y.; Liu, D.; You, T. Hierarchically porous $NiCo_2S_4$ nanowires anchored on flexible electrospun graphitic nanofiber for high-performance glucose biosensing. *J. Alloys Compd.* **2020**, *819*, 153376. [CrossRef]
20. Wang, A.; Feng, J.; Li, Z.; Liao, Q.; Wang, Z.; Chen, J. Solvothermal synthesis of Cu/Cu_2O hollow microspheres for non-enzymatic amperometric glucose sensing. *CrystEngComm* **2012**, *14*, 1289–1295. [CrossRef]
21. Li, M.; Zhao, Z.; Liu, X.; Xiong, Y.; Han, C.; Zhang, Y.; Bo, X.; Guo, L. Novel bamboo leaf shaped CuO nanorod@hollow carbon fibers derived from plant biomass for efficient and nonenzymatic glucose detection. *Analyst* **2015**, *140*, 6412–6420. [CrossRef] [PubMed]
22. Yin, H.; Zhu, J.; Chen, J.; Gong, J.; Nie, Q. Hierarchical $CuCo_2O_4/C$ microspheres assembled with nanoparticle-stacked nanosheets for sensitive non-enzymatic glucose detection. *J. Mater. Sci.* **2018**, *53*, 11951–11961. [CrossRef]
23. Xu, H.; Han, F.; Xia, C.; Wang, S.; Zhuiykov, S.; Zheng, G. Spinel sub-stoichiometric $Cu_xCo_yO_4$ nano-wire framework thin-film electrode for enhanced electrochemical non-enzymatic sensing of glucose. *Electrochim. Acta* **2020**, *331*, 135295. [CrossRef]
24. Zhang, X.; Wang, G.; Gu, A.; Wei, Y.; Fang, B. CuS nanotubes for ultrasensitive nonenzymatic glucose sensors. *Chem. Commun.* **2008**, 5945–5947. [CrossRef] [PubMed]
25. Karikalan, N.; Karthik, R.; Chen, S.; Karuppiah, C.; Elangovan, A. Sonochemical synthesis of sulfur doped reduced Graphene oxide supported CuS nanoparticles for the non-enzymatic glucose sensor applications. *Sci. Rep.* **2017**, *7*, 2494. [CrossRef] [PubMed]
26. Xu, W.; Lu, J.; Huo, W.; Li, J.; Wang, X.; Zhang, C.; Gu, X.; Hu, C. Direct growth of $CuCo_2S_4$ nanosheets on carbon fiber textile with enhanced electrochemical pseudocapacitive properties and electrocatalytic properties towards glucose oxidation. *Nanoscale* **2018**, *10*, 14304. [CrossRef]
27. Zhan, W.; Sun, L.; Han, X. Recent Progress on Engineering Highly Efficient Porous Semiconductor Photocatalysts Derived from Metal–Organic Frameworks. *Nano-Micro Lett.* **2019**, *11*, 1. [CrossRef]
28. Li, Y.; Xu, Y.; Yang, W.; Shen, W.; Xue, H.; Pang, H. MOF-Derived Metal Oxide Composites for Advanced Electrochemical Energy Storage. *Small* **2018**, *14*, 1704435. [CrossRef]
29. Salunkhe, R.; Kaneti, Y.; Yamauchi, Y. Metal−Organic Framework- Derived Nanoporous Metal Oxides toward Supercapacitor Applications: Progress and Prospects. *ACS Nano* **2017**, *11*, 5293–5308. [CrossRef]
30. Cai, Z.; Wang, Z.; Kim, J.; Yamauchi, Y. Hollow Functional Materials Derived from Metal–Organic Frameworks: Synthetic Strategies, Conversion Mechanisms, and Electrochemical Applications. *Adv. Mater.* **2019**, *31*, 1804903. [CrossRef]
31. Long, L.; Liu, X.J.; Chen, L.L.; Wang, S.Y.; Liu, M.C.; Jia, J.B. MOF-derived 3D leaf-like CuCo oxide arrays as an efficient catalyst for highly sensitive glucose detection. *Electrochim. Acta* **2019**, *308*, 243–252. [CrossRef]
32. Luo, Y.; Wang, Q.; Li, J.; Xu, F.; Sun, L.; Bu, Y.; Zou, Y.; Kraatz, H.; Rosei, F. Tunable hierarchical surfaces of CuO derived from metal–organic frameworks for non-enzymatic glucose sensing. *Inorg. Chem. Front.* **2020**, *7*, 1512–1525. [CrossRef]
33. Shu, Y.; Yan, Y.; Chen, J.; Xu, Q.; Pang, H.; Hu, X. Ni and NiO Nanoparticles Decorated Metal−Organic Framework Nanosheets: Facile Synthesis and High-Performance Nonenzymatic Glucose Detection in Human Serum. *ACS Appl. Mater. Interfaces* **2017**, *9*, 22342–22349. [CrossRef] [PubMed]
34. Kim, K.; Kim, S.; Lee, H.; Park, Y.; Bae, Y.; Kim, H. Electrochemically derived CuO nanorod from copper-based metal-organic framework for non-enzymatic detection of glucose. *Appl. Surf. Sci.* **2019**, *479*, 720–726. [CrossRef]
35. Xiao, Z.; Bao, Y.; Li, Z.; Huai, X.; Wang, M.; Liu, P.; Wang, L. Construction of Hollow Cobalt−Nickel Phosphate Nanocages through a Controllable Etching Strategy for High Supercapacitor Performances. *ACS Appl. Energy Mater.* **2019**, *2*, 1086–1092. [CrossRef]
36. Zhang, D.J.; Zhang, J.C.; Shi, H.Z.; Guo, X.L.; Guo, Y.Y.; Zhang, R.C.; Yuan, B.Q. Redox-active microsized metal-organic framework for efficient nonenzymatic H_2O_2 sensing. *Sens. Actuators B* **2015**, *221*, 224–229. [CrossRef]
37. Kang, L.; Huang, C.; Zhang, J.; Zhang, M.Y.; Zhang, N.; Liu, S.D.; Ye, Y.; Luo, C.; Gong, Z.W.; Wang, C.L.; et al. Effect of fluorine doping and sulfur vacancies of $CuCo_2S_4$ on its electrochemical performance in supercapacitors. *Chem. Eng. J.* **2020**, *390*, 124643. [CrossRef]
38. Han, X.Z.; Qin, Y.; Luo, J.X.; Zhang, F.Z.; Lei, X.D. Polygonal CuS Nanoprisms Fabricated by Grinding Reaction for Advanced Quasi-Solid-State Asymmetry Supercapacitors. *ACS Appl. Energy Mater.* **2021**, *4*, 12631–12640. [CrossRef]
39. Fan, S.; Zhao, M.; Ding, L.; Liang, J.; Chen, J.; Li, Y.; Chen, S. Synthesis of 3D hierarchical porous Co_3O_4 film by eggshell membrane for non-enzymatic glucose detection. *J. Electroanal. Chem.* **2016**, *775*, 52–57. [CrossRef]
40. Li, S.; Hou, L.; Yuan, B.; Chang, M.; Ma, Y.; Du, J. Enzyme-free glucose sensor using a glassy carbon electrode modified with reduced graphene oxide decorated with mixed copper and cobalt oxides. *Microchim. Acta* **2016**, *183*, 1813–1821. [CrossRef]

41. Li, Y.; Zhong, Y.; Zhang, Y.; Weng, W.; Li, S. Carbon quantum dots/octahedral Cu_2O nanocomposites for non-enzymatic glucose and hydrogen peroxide amperometric sensor. *Sens. Actuators B* **2015**, *206*, 735–743. [CrossRef]
42. Liu, X.; Yang, Y.; Liu, R.; Shi, Z.; Ma, L.; Wei, M. Synthesis of porous CuO microspheres assembled from (001) facetexposed nanocrystals with excellent glucose-sensing performance. *J. Alloys Compd.* **2017**, *718*, 304–310. [CrossRef]
43. Yang, J.; Cho, M.; Lee, Y. Synthesis of hierarchical $NiCo_2O_4$ hollow nanorods via sacrificial-template accelerate hydrolysis for electrochemical glucose oxidation. *Biosens. Bioelectron.* **2016**, *75*, 15–22. [CrossRef] [PubMed]